Rashba-like spin splitting around non-time-reversal-invariant momenta

L. L. Tao,[1,][*] Jiayu Li [ORCID],[2] Yuntian Liu,[2] Xianjie Wang,[1] Yu Sui,[1] Bo Song,[3] M. Ye. Zhuravlev [ORCID],[4] and Qihang Liu [ORCID][2,][†]

[1]*School of Physics, Harbin Institute of Technology, Harbin 150001, China*
[2]*Shenzhen Institute for Quantum Science and Engineering and Department of Physics,*
Southern University of Science and Technology, Shenzhen 518055, China
[3]*National Key Laboratory of Science and Technology on Advanced Composites in Special Environments,*
Harbin Institute of Technology, Harbin 150001, China
[4]*St. Petersburg State University, St. Petersburg 190000, Russia*

The ubiquitous Rashba spin splitting occurring around time-reversal-invariant momenta (TRIM) reflects the fundamental interplay between spin-orbit coupling (SOC) and crystalline symmetry. Unexpectedly, recent measurements reveal novel Rashba spin splitting around the momenta lacking time-reversal symmetry (non-TRIM), whose mechanism remains elusive. Here, we theoretically elucidate the microscopic origin of Rashba spin splitting around non-TRIM and identify the design principles for its appearance. Conventionally, a Zeeman-like spin splitting dominates around non-TRIM due to the broken time-reversal symmetry and diminishes the Rashba-like features. Our results show that the Bloch wave function with specific orbital representation at certain non-TRIM could eliminate the first-order SOC effect. As a result, the corresponding little group hosts a type of quasisymmetry that commutes with the dominating SOC Hamiltonian, leading to a tiny SOC gap and helical spin texture. Furthermore, such a quasi-symmetry-induced tiny gap could manifest large Berry curvature, which is desirable for various topological applications. Our work expands the concept of Rashba physics beyond the conventional TRIM scenario, paving an avenue for designing novel spin-splitting materials through the cooperation of symmetry and orbital engineering.

I. INTRODUCTION

One of the central phenomena of spin-orbit coupling (SOC) in nonmagnetic crystals without inversion symmetry is the spin splitting (SS), i.e., energy separation of the spins with opposite directions, as demonstrated by Dresselhaus [1] and Rashba [2]. The resultant spin-polarized energy bands manifest various spin textures, i.e., the expectation value of the spin operators on a Bloch state, in momentum space. Depending on the specific wave vector $\mathbf{k}_0$, the SS around the $\mathbf{k}_0$ point may exhibit different types of spin textures such as Rashba, Dresselhaus, Zeeman, Weyl, persistent, and so on [1–5], giving rise to fertile possibilities for next-generation spintronics. For example, Rashba SS manifesting a helical spin texture has aroused considerable interest due to its fundamental interest and promising applications [6,7] such as spin field effect transistors [8,9], Edelstein effect (charge-to-spin conversion) [10], and topological superconductivity [11,12]. Equal contributions of Rashba and Dresselhaus SOC result in a unidirectional spin-orbit field and the so-called persistent spin texture [13–17], which preserves a hidden SU(2) symmetry rendering an ultimately infinite spin lifetime [13,14]. Weyl-type spin texture reveals a hedgehog spin configuration,

which is reminiscent of a magnetic monopole in momentum space [18–20].

From the symmetry point of view, the SS occurring around a specific wave vector $\mathbf{k}_0$ is dictated by the little group of $\mathbf{k}_0$. More importantly, the time-reversal symmetry $\mathcal{T}$ of the little group also plays an essential role in determining the spin-texture types [6,7]. For example, Rashba SS (or Dresselhaus SS) occurs at $\mathbf{k}_0$ that is a time-reversal invariant momentum (TRIM) [6], where the doubly degeneracy at $\mathbf{k}_0$ is protected by Kramers theorem [$\Delta E(\mathbf{k}_0) = 0$; see Fig. 1(a)]. In sharp contrast, Zeeman-type SS [3,21,22] happens at non-TRIM with $\Delta E(\mathbf{k}_0) > 0$, as shown in Fig. 1(b). It is generally expected that the Zeeman-like SOC features will diminish the Rashba-like features around non-TRIM. These features establish the current textbook *Gestalt* underlying our understanding of SS's in nonmagnetic materials.

Interestingly, recent studies have shown unconventional Rashba SS appearing at the non-TRIM [23–26], implying that time-reversal symmetry of the little group may not be a necessary condition for Rashba SS [23]. For example, based on the spin- and angle-resolved photoelectron spectroscopy (ARPES) measurements, Rashba SS was reported around the non-TRIM K point (little group C_{3v} symmetry) of the Bi monolayer absorbed on an Si(111) surface, i.e., β-Bi/Si(111)-$\sqrt{3} \times \sqrt{3}$ surface [23], evidenced by the observed band's degeneracy at K within the resolution of ARPES [$\Delta E(\mathbf{k}_0) \approx 0$] and a helical spin texture [see Fig. 1(c)]. The observed degeneracy was attributed to the fact that the $p31m$

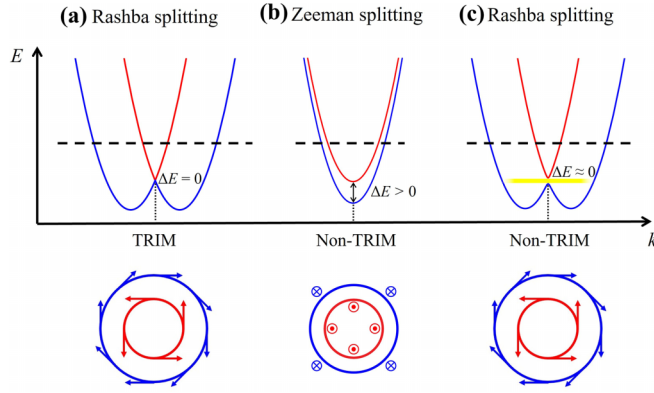[*]lltao@hit.edu.cn
[†]liuqh@sustech.edu.cn

FIG. 1. Top: Sketches of SS bands around TRIM (e.g., Γ) and non-TRIM (e.g., K), as indicated by vertical dashed lines. Red and blue colors represent two SS branches for (a) Rashba type, (b) Zeeman type, and (c) Rashba-Zeeman type. The bands are Kramers degenerate and SS at the TRIM and non-TRIM, respectively. Bottom: Schematic spin textures at Fermi contours. It is to be noted that in (b) and (c), there is another non-TRIM point related by time-reversal symmetry $\mathcal{T}$ with opposite SS and spin texture.

layer group with little group C_{3v} of K can produce a two-dimensional representation to ensure the exact degeneracy of the splitting bands at non-TRIM [25]. More surprisingly, a recent spin-resolved ARPES work has shown that Rashba-type and Zeeman-type SS's coexist in different bands around the non-TRIM K point for the Sn/SiC(0001)-1 × 1 surface [26], where the little group C_3 of K only has one-dimensional representation. It was explained that the types of SS are determined by the distinct symmetries of K based on the charge density distributions of different bands, which is seemingly inconsistent with the traditional symmetry argument that the little group symmetry of the same wave vector is unique [32]. Such coincident SS features that require preserved $\mathcal{T}$ and broken $\mathcal{T}$ pose the origin of Rashba SS around non-TRIM as an open question in understanding the symmetry-related SS.

In this work, using symmetry analysis and density functional theory (DFT) calculations, we reveal the microscopic mechanism responsible for Rashba-like SS around non-TRIM and identify the design principles for its occurrence. Exemplified by the Sn/SiC(0001)-1 × 1 surface, we show that despite broken $\mathcal{T}$ symmetry at the K point, for certain C_3 representations that eliminate the first-order SOC effect, there exists a type of spin-rotation quasisymmetry [27,28] that commutes with the dominant SOC Hamiltonian, but not with the high-order perturbation term. In Ref. [28], a near-degenerate nodal plane (tiny gap below 2 meV) in semimetal CoSi is formed owing to quasisymmetry, which in turn results in the large Berry curvatures. Similarly, in our work, the realization of spin-rotation quasisymmetry leads to a tiny SOC gap. As a result, such quasisymmetry leads to a tiny SOC gap invisible by ARPES as well as helical spin texture [Fig. 1(c)]. Our design principle further provides all the possible little groups of $\mathbf{k}_0$ and the corresponding representations that support Rashba SS around non-TRIM. Our work expands the concept of Rashba physics beyond the conventional TRIM scenario, paving an avenue for designing novel spin-splitting materials through the cooperation of symmetry and orbital engineering.

II. COMPUTATIONAL METHOD AND DETAILS

Our density functional theory (DFT) calculations were performed using the plane-wave ultrasoft pseudopotential method [29], as implemented in QUANTUM ESPRESSO [30]. An energy cutoff of 544 eV for the plane-wave expansion, generalized gradient approximation (GGA) [31] for the exchange and correlation functional, and a $10 \times 10 \times 1$ k-point mesh for the self-consistent calculations were adopted throughout. The atomic coordinators were fully relaxed with the force tolerance of 2.6 meV/Å. The Sn/SiC(0001)-1 × 1 surface consists of monolayer Sn on the top site of 6H-SiC(0001) with six bilayers and the in-plane lattice was fixed as 3.081 Å. The Tl/Si(111)-1 × 1 surface consists of monolayer Tl at the T_4 site of the Si(111) substrate with six bilayers and the in-plane lattice was fixed as 3.840 Å. The Bi/Si (111)-$\sqrt{3} \times \sqrt{3}$ surface consists of monolayer Bi at the T_4 site of the Si(111) substrate with three bilayers and the in-plane lattice was fixed as 6.650 Å. For all surface systems, the bottom surface is saturated with hydrogen atoms and a vacuum region of 15 Å along the z direction is imposed.

III. RASHBA SS AROUND NON-TRIM

We first revisit the Sn/SiC(0001)-1 × 1 surface, which was recently investigated by spin-resolved ARPES [26], and elucidate the origin of observed *peculiar* SS's. As shown in Figs. 2(a) and 2(b), the Sn/SiC(0001) surface consists of monolayer Sn at the top site of the 6H-SiC(0001) substrate and the crystallographic point group (PG) is C_{3v} (containing three vertical mirror planes M_{100}, M_{010}, M_{110} and one three-fold rotation axis C_{3z}). The corresponding space group (SG) is thus $P3m1$ and the little group of K is C_3. From the DFT results shown in Fig. 2(d), we observe two completely different SS's around the Fermi level: a sizable SS (157 meV) for S1 bands, while a negligible SS (2 meV) for S2 bands at the same non-TRIM K, consistent with the previous measurement [26]. Spin textures around K for the lower branch of SS bands, shown in Fig. 2(e), further reveal a Zeeman (Rashba) type for S1 (S2) bands. Compared with the common Zeeman-type SS of the S1 band, the Rashba SS of the S2 band around non-TRIM K is unexpected. Such *unconventional* Rashba SS at K was attributed to the C_{3v} symmetry of the charge density of the S2 band, rather than the little group C_3 of K [26], which is somehow puzzling because the PG symmetry is only wave-vector dependent [32] and PGs of S1 and S2 Bloch states at K should both be C_3. In the following, we will explain these results from the perspective of orbital representation and quasisymmetry.

We start from the general SOC Hamiltonian around the $\mathbf{k}_0$ point with little group $G_{\mathbf{k}_0}$, which can be written as [33]

$$H_{SOC} = H_0 + H(\mathbf{k}), \qquad (1)$$

where the first (second) term is k independent (k dependent). H_0 is the first-order atomic SOC given by $\lambda \mathbf{L} \cdot \mathbf{S}$, where $\mathbf{L}$ ($\mathbf{S}$) is the orbital (spin) angular momentum operator and λ is the intra-atomic SOC constant. Since H_0 can be obtained by
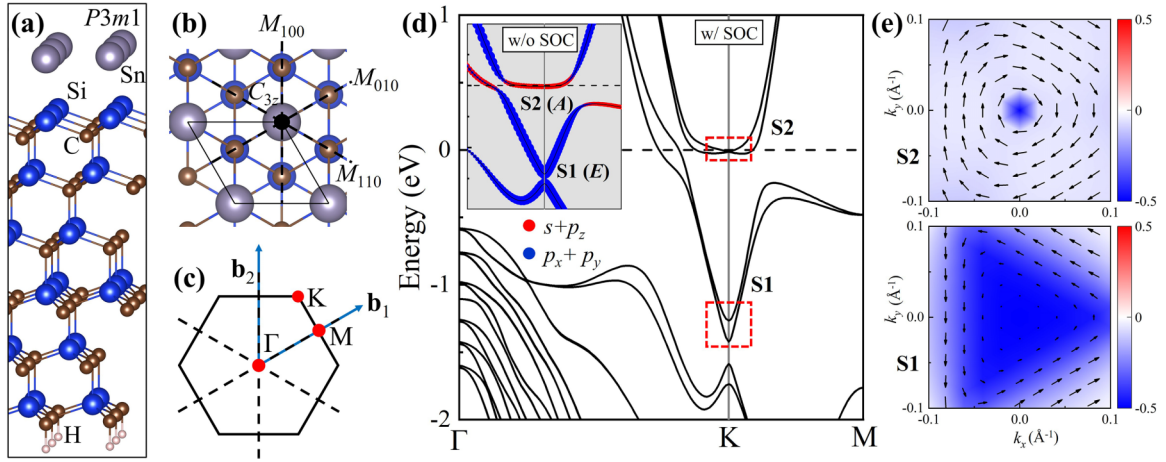
FIG. 2. (a),(b) Atomic structure of the Sn/SiC(0001)-1×1 surface with top adsorption site, namely, the site above the surface Si atoms, where M_{100}, M_{010}, and M_{110} denote the mirror planes, while C_{3z} denotes the threefold rotation axis. (c) First Brillouin zone (BZ), where Γ (0, 0), M (1/2, 0), and K (1/3, 1/3). Dashed lines denote the mirror planes. The reciprocal primitive vectors $\mathbf{b}_{1,2}$ are given by $\mathbf{b}_1 = \frac{2\pi}{a}\hat{x} + \frac{2\pi}{\sqrt{3}a}\hat{y}$, $\mathbf{b}_2 = \frac{4\pi}{\sqrt{3}a}\hat{y}$, where a is the lattice constant. (d) Band structure with SOC. Inset: Orbital-projected band structure onto Sn-s, p orbitals around K without SOC. The Fermi level is aligned to zero, as indicated by the dashed lines. (e) Spin textures around K for the lower branch of S1 and S2 bands as highlighted by red boxes in (d). The in-plane spin components s_x and s_y are shown by arrows, while the out-of-plane spin component s_z is indicated by color.

calculating the expectation value of the $\mathbf{L}$ operator on a given Bloch function $u_{\mathbf{k}}(\mathbf{r})$, namely, $H_0 \sim \langle u_{\mathbf{k}}|\mathbf{L}|u_{\mathbf{k}}\rangle$, it is expected to be sizable when the expectation value of $\mathbf{L}$ is large and not quenched [33]. The k-dependent term $H(\mathbf{k})$ can be written as $H(\mathbf{k}) = \mathbf{\Omega}(\mathbf{k}) \cdot \boldsymbol{\sigma}$ [40], where the wave vector $\mathbf{k}$ is measured from $\mathbf{k}_0$ and $\boldsymbol{\sigma} = (\sigma_x, \sigma_y, \sigma_z)$ are the Pauli matrices operating on the spin eigenstates $|\pm\frac{1}{2}\rangle$. As shall be discussed, $H(\mathbf{k})$ is determined by $G_{\mathbf{k}_0}$. In general, the type of SS around the $\mathbf{k}_0$ point is depicted by Eq. (1). For TRIM $\mathbf{k}_0$, H_0 is zero and the type of SS is depicted by $H(\mathbf{k})$. For non-TRIM $\mathbf{k}_0$, when H_0 dominates over $H(\mathbf{k})$, the SS around $\mathbf{k}_0$ is the Zeeman type characterized with parabolalike bands. For non-TRIM $\mathbf{k}_0$, when the SU(2) quasisymmetry is present (as shall be shown next) and the Rashba term $\alpha(k_x\sigma_y - k_y\sigma_x)$ in $H(\mathbf{k})$ dominates over other terms, the gap at $\mathbf{k}_0$ is tiny and such SS is defined as the Rashba-like type. As seen from Fig. 1(c), Rashba-like SS is characterized by the W-shaped band crossing and helical spin texture.

For the case of the Sn/SiC(0001)-1×1 surface, the little group of K is C_3, which has three one-dimensional irreducible representations [32]. Based on the symmetry analysis and orbital projection from DFT, we construct the symmetry-adapted basis functions for S1 (E representation) and S2 bands (A representation) as follows:

$$|\phi_E^\tau\rangle = -\frac{1}{\sqrt{2}}(\tau|p_x\rangle + i|p_y\rangle), \quad |\phi_A\rangle = |p_z\rangle, \quad (2)$$

where p denotes the atomic orbitals of Sn, and $\tau = \pm 1$ is the valley index and the two valleys are related by $\mathcal{T}$. Specifically, the S1 and S2 Bloch states at K belong to E and A representations, respectively [without SOC; inset of Fig. 2(d)]. From Eq. (1), we can obtain $\langle\phi_A|\lambda\mathbf{L}\cdot\mathbf{S}|\phi_A\rangle = 0$ and $\langle\phi_E^\tau|\lambda\mathbf{L}\cdot\mathbf{S}|\phi_E^\tau\rangle = \lambda\tau\sigma_z$, indicating that the gap of the S2 band at K is opened by the higher-order effect of SOC, but the gap of the S1 band is opened by the first-order one.

Beyond the orbital representation, the reason for the tiny gap of 2 meV for the S2 band at K compared with that of the S1 band (157 meV) is the protection of quasisymmetry [27,28]. Counting the spin degree of freedom, without SOC the little group of K is $C_3 \otimes$ SU(2) [34], where the spin-rotation group SU(2) is generated by spin rotation along three axes $U_\alpha(\phi)$ ($\alpha = x, y, z$ and ϕ is infinitesimal angle). The SU(2) symmetry ensures the double degeneracy of the energy bands at any momenta. With SOC, the symmetry of K is then lowered to the double group C_3^D as the spin rotations are fully coupled to the spatial rotations. The spin degeneracy of both A and E representations of the single group will split due to the spin-up and -down channels carrying different representations of the double group. One can verify that the general $H_0 \propto \sigma_z$ does not commute with spin rotation $U_{x,y}(\phi) = \exp(-i\phi\sigma_{x,y}/2)$; then the spin rotation along the in-plane axis is not the symmetry of any Bloch state at K. However, if integrating out the remote bands near the Fermi energy and projecting the atomic SOC down to the A or E representation, we obtain the effective atomic SOC term up to the first order for A and E representations, which is $H_0^{A(1)} = 0$ and $H_0^{E(1)} = \lambda\sigma_z$, respectively. Distinct from the case of E representation with $[H_0^{E(1)}, U_{x,y}(\phi)] \neq 0$, the first-order SOC term of A representation commutes with the in-plane spin rotation $[H_0^{A(1)}, U_{x,y}(\phi)] = 0$, while the commutation becomes nonzero for the second-order term $H_0^{A(2)} \propto \lambda^2\sigma_z$. Hence, the spin-rotation quasisymmetry $U_{x,y}(\phi)$ of the first-order SOC term of A representation combined with the spin-rotation along the z axis generate a SU(2) quasisymmetry, which protects the near degeneracy at K of $\Delta E(K) \approx 0$.

For a more transparent demonstration, based on the above analysis of orbital representation and quasisymmetry, we express H_0 as

$$H_0 = \frac{\lambda}{2}\tau(\mu + 1)\sigma_z, \quad (3)$$

TABLE I. The little group G_K of the K point and symmetry-allowed SOC terms $H(k)$ (linear order in k measured from K) for different PGs and SGs without inversion symmetry. Trigonal crystal system contains the PGs C_3, D_3, and C_{3v}, while the hexagonal one contains the PGs C_6, D_6, and C_{6v}. The second column represents the representations with negligible atomic SOC, while the symmetry-adapted basis functions are given in parentheses. For $H(k)$, R and W represent the Rashba SOC $k_x\sigma_y - k_y\sigma_x$ and Weyl SOC $k_x\sigma_x + k_y\sigma_y$, respectively, while R+W represents the coexistence of Rashba and Weyl SOCs.

PG (SG)	Representations	G_K	$H(\mathbf{k})$
C_3 ($P3$)	A (p_z, $d_{x^2+y^2}$, d_{z^2})	C_3	R+W
D_3 ($P312$)	A (p_z, $d_{x^2+y^2}$, d_{z^2})	C_3	R+W
D_3 ($P321$)	A_1 ($d_{x^2+y^2}$, d_{z^2}), A_2 (p_z)	D_3	W
C_{3v} ($P3m1$)	A (p_z, $d_{x^2+y^2}$, d_{z^2})	C_3	R+W
C_{3v} ($P31m$)	A_1 (p_z, $d_{x^2+y^2}$, d_{z^2})	C_{3v}	R
C_6 ($P6$)	A (p_z, $d_{x^2+y^2}$, d_{z^2})	C_3	R+W
D_6 ($P622$)	A_1 ($d_{x^2+y^2}$, d_{z^2}), A_2 (p_z)	D_3	W
C_{6v} ($P6mm$)	A_1 (p_z, $d_{x^2+y^2}$, d_{z^2})	C_{3v}	R

where $\mu = +1$ (-1) for E (A) representation. Constrained by the PG C_3, the k-dependent term $H(\mathbf{k})$ contains the Rashba- and Weyl-type SOC (see Table I, discussed later). Unlike the distinct order effects dominating the completely different gaps at K of S1 and S2 bands, the first-order effect of the k-dependent SOC term is the leading order for both A and E representations for finite $\mathbf{k}$ around K. Thus, $H(\mathbf{k})$ of both representations break in-plane spin rotation entirely, leading to a first-order SS around K. Therefore, the SOC Hamiltonian around K up to linear order in k for the Sn/SiC(0001)-1 × 1 surface reads

$$H_{RWZ} = \frac{\lambda}{2}\tau(\mu + 1)\sigma_z + \alpha(k_x\sigma_y - k_y\sigma_x) + \beta(k_x\sigma_x + k_y\sigma_y),$$

(4)

where the first term is the Zeeman (Z) SOC, the second and third terms represent the Rashba (R) and Weyl (W) types SOC, respectively, and α and β are independent SOC parameters. With the sharp contrast between the leading order of H_0 and $H(\mathbf{k})$, the S2 band of A representation produces the unconventional SS at non-TRIM K, since the Rashba-Weyl term dominates over the tiny Zeeman term protected by SU(2) quasisymmetry. This also accounts for the observed in-plane helical spin texture around the K point for S2 bands [see Fig. 2(d)] and the tiny gap of 2 meV in general is invisible from the ARPES measurements due to the energy resolution [26]. Conversely, a Zeeman SS dominates around K for S1 bands because the first-order effect of atomic SOC does not vanish for E representation, and the spin texture is mainly out of plane. Therefore, although pure spin rotation is apparently not an exact symmetry of the system with SOC, the existence of SU(2) quasisymmetry for certain representations still manifests approximate degeneracy at non-TRIM and thus Rashba-like SS.

To further confirm our symmetry analysis, we revisit another example, namely, a Tl/Si(111)-1 × 1 surface, as shown in Fig. 3(a), which is composed of monolayer Tl at
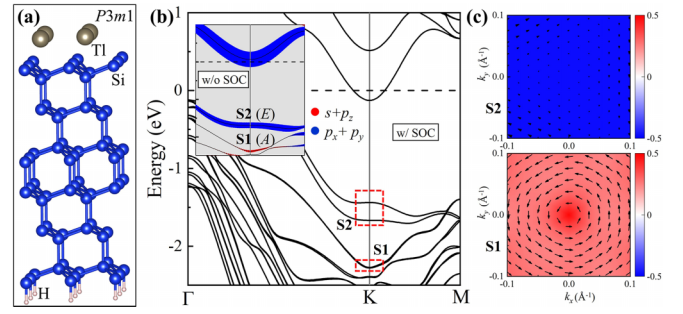

FIG. 3. (a) Atomic structure of the Tl/Si(111)-1 × 1 surface with the T_4 adsorption site, namely, the site above the second-layer atoms from the surface. (b) Band structure with SOC. Inset: Orbital-projected band structure onto Tl-s, p orbitals around K without SOC. (c) Spin textures around K for the lower branch of the S1 and S2 bands as highlighted by red boxes in (b).

the T_4 site of the Si(111) substrate. A sizable Zeeman-type SS at the K point has been reported by spin-resolved ARPES measurements [35]. The crystallographic PG and SG for the Tl/Si(111)-1 × 1 surface are C_{3v} and $P3m1$, respectively, which are the same as that of the Sn/SiC(0001)-1 × 1 surface. As seen from Fig. 3(b), S1 bands composed mainly of a Tl-s, p_z orbital (A representation) reveal a tiny SS (6 meV), while S2 bands composed mainly of Tl-p_x, p_y orbitals (E representation) exhibit a sizable SS (229 meV) at K. The spin textures shown in Fig. 3(c) also exhibit a pure Zeeman type for S2 bands and a Rashba-Zeeman type for S1 bands. We note that the sizable Zeeman-type SS of over 100 meV at K was also demonstrated in monolayer transition-metal dichalcogenides [36], in which the little group of K (C_{3h}) forbids the linear k-dependent SOC. Thus, monolayer transition metal dichalcogenides sustain the pure Zeeman-type SS around the K point. Furthermore, the Sn/SiC(0001)-1 × 1 and Tl/Si(111)-1 × 1 surfaces are metallic systems with sizable SS's around the Fermi levels. Thus, one can explore the spin-transport properties such as current-induced spin polarization [37] and spin Hall effect, as recently explored for the Pb/SiC(0001)-1 × 1 surface system [38].

IV. DESIGN PRINCIPLES

Next, we will perform a general symmetry analysis and establish the design principle for the Rashba-like SS around non-TRIM. As demonstrated in Eq. (1), the SOC Hamiltonian contains the atomic and k-dependent terms. The absence of the atomic term H_0 relies on certain representations and atomic orbital components. The k-dependent term $H(k) = \mathbf{\Omega}(\mathbf{k}) \cdot \boldsymbol{\sigma}$ can be determined from the following symmetry constraints [39,40]:

$$\mathbf{\Omega}(\mathbf{k}) = \det(g)g^{-1}\mathbf{\Omega}(g\mathbf{k}),$$

(5)

where the symmetry operation $g \in G_{\mathbf{k}_0}$ and $\det(g) = +1$ (-1) for proper (improper) rotations. By using the method of invariants [39–43], we calculated $\mathbf{\Omega}(\mathbf{k})$ (linear order in k) around non-TRIM K for different PGs and SGs, as listed in Table I. Part of them have also been reported by previous work [4,40]. Here we consider the trigonal and hexagonal crystal systems and limit our consideration to two

dimensions and symmorphic SGs. It is to be noticed that R and W represent the Rashba SOC $k_x\sigma_y - k_y\sigma_x$ and Weyl SOC $k_x\sigma_x + k_y\sigma_y$, respectively, while R + W represents the coexistence of Rashba and Weyl SOCs. We first note that the wave vector PG is SG dependent—for example, the PG at K is C_3 (D_3) for SG $P312$ ($P321$). This suggests that only crystallographic PG is insufficient to describe the electronic properties and spin structures in momentum space. On the other hand, although the similar symmetry analysis based on invariant theory has also been demonstrated by previous work [4,40], most previous studies focus on the k-dependent SOC $H(\mathbf{k})$ around $\mathbf{k}_0$ [4,40], which is directly determined by the little group $G_{\mathbf{k}_0}$. In the case of non-TRIM $\mathbf{k}_0$, this is just part of the picture and the whole picture should also consider the atomic SOC H_0, which is representation dependent.

We now move to the establishment of the design principle for the Rashba-like SS around non-TRIM. As mentioned earlier, Rashba SS is characterized by two distinct features [2,6,7]: approximate degeneracy and helical spin textures, as shown in Fig. 1(c). To satisfy the approximate degeneracy at non-TRIM, the atomic SOC [first term in Eq. (1)] should be negligible, suggesting that the Bloch state belongs to a certain representation as listed in the second column of Table I, e.g., A representation for PG C_3. To satisfy the helical spin textures around the $\mathbf{k}_0$ point, the ideal case is that only the Rashba term $\alpha(k_x\sigma_y - k_y\sigma_x)$ exists in $H(\mathbf{k})$ of Eq. (1), suggesting that the little group $G_{\mathbf{k}_0}$ should be C_{3v} [44], C_{4v} [45–47], D_6, and C_{6v} [48]. From Table I, only SGs $P31m$ and $P6mm$ have PG C_{3v} at the non-TRIM K, which sustains the helical spin textures. Thus, for trigonal and hexagonal crystal systems, the combination of SG $P31m$ or $P6mm$ and the Bloch state with A_1 representation sustains the Rashba-like SS around the K point. Generally, the Zeeman-like term dominates around the non-TRIM [3,21,22] because a sizable Zeeman SOC overwhelms the Rashba-like features. However, as demonstrated in this work, the quasisymmetry for certain orbital representation leads to a tiny Zeeman-like gap, such that W-shaped band crossing and helical spin texture features are still dominant.

To confirm this, we revisit the Bi/Si(111)-$\sqrt{3} \times \sqrt{3}$ surface system, as shown in Fig. 4(a), which consists of monolayer Bi at the T_4 site of the Si(111) substrate [24]. The SG is $P31m$ and the PG of K is thus C_{3v}. According to Table I, the linear SOC Hamiltonian is Rashba type, while the atomic SOC is representation dependent. This is exactly in accordance with our DFT results. As seen from Fig. 4(b), the bands (red boxes) composed mainly of Bi-s, p_z orbitals (A_1 representation, inset) reveal a Rashba-type band crossing around K. In addition, the calculated spin textures shown in Fig. 4(c) exhibit a perfect helical type. Therefore, the formation of Rashba-like SS around non-TRIM requires the selected little group symmetry as well as the orbital representation. Such principles also apply to the recently reported quantum spin Hall candidate, i.e., bismuthene on SiC substrate [49], where similar spin-splitting dispersion is observed around the K point.

V. DISCUSSION AND SUMMARY

Having discussed the mechanism and design principles, we next move to the possible applications of Rashba-like
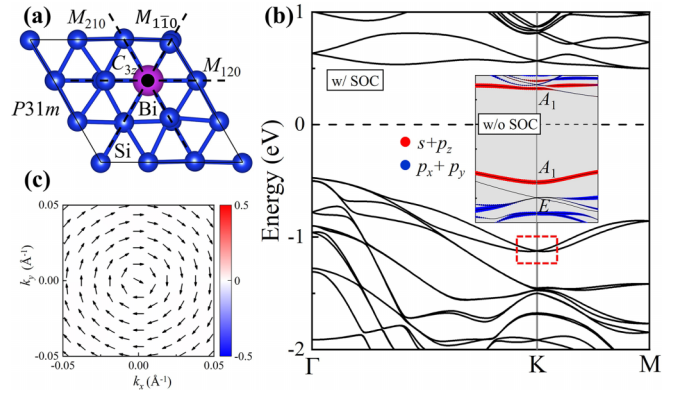

FIG. 4. (a) Top view of the Bi/Si(111)-$\sqrt{3} \times \sqrt{3}$ surface with the T_4 adsorption site, namely, the site above the second-layer atoms from the surface. (b) Band structure with SOC. Inset: Orbital-projected band structure onto Bi-s, p orbitals around K without SOC. (c) Spin textures around K for the lower branch of bands as highlighted by red boxes in (c).

SS around non-TRIM. One example is the large Berry curvature induced by the quasi-symmetry-protected tiny SOC gap [27,50]. It is to be noted that the idea of a quasi-symmetry-protected tiny gap responsible for large Berry curvatures has been demonstrated in the semimetal CoSi [27,28]. To explicitly illustrate this, we use the Rashba-Zeeman (RZ) SOC Hamiltonian, namely, $H_{RZ} = \alpha(k_x\sigma_y - k_y\sigma_x) + \Delta E/2\sigma_z$, where ΔE quantifies the tiny gap for the Rashba-like SS. One can calculate the Berry curvature $\mathbf{\Omega}$ as [50]

$$\Omega_z^{\pm} = \pm \frac{\Delta E \alpha^2}{4(\alpha^2 k^2 + \Delta E^2/4)^{3/2}}. \tag{6}$$

In the case of conventional Rashba SS with $\Delta E = 0$ at TRIM, Berry curvatures around TRIM vanish due to the combination of time-reversal symmetry and continuous rotation symmetry about the z axis [50]. In sharp contrast, the Rashba-like SS around non-TRIM reveals large Berry curvatures due to the quasi-symmetry-protected tiny gap ΔE, as seen from $\Omega(k = 0) \propto 1/\Delta E^2$. Noteworthy is the fact that the Berry curvatures are opposite between two non-TRIM points related by time-reversal symmetry and the integral of the Berry curvature responsible for the anomalous Hall effect is thus zero. One could explore the valley Hall effect when the two non-TRIM points K and $-K$ can be regarded as valleys from band dispersion [36,50]. In addition, it is instructive to compare the large Berry curvature between the Rashba-Zeeman and Weyl node. As seen from Table II, the Berry curvature for the 3D Weyl node diverges and reveals a hedgehog configuration around the node. In contrast, the Berry curvature for Rashba-Zeeman is finite at non-TRIM.

We also note that under a built-in electric field, the distribution of the Berry curvature in spatial inversion broken systems may lead to exotic phenomena such as the Magnus Hall effect [51], Magnus Nernst/thermal Hall effect [52], and Magnus spin Nernst/thermal effect [53]. More importantly, it is recently reported that in gapped Rashba systems, both the Magnus electronic, spin, and spin Nernst conductivities produce a higher peak as the gap gets smaller [53]. Thus,

TABLE II. Comparison of Hamiltonian and Berry curvature $\boldsymbol{\Omega}$ between different models. v is the Fermi velocity.

Model	Hamiltonian	$\boldsymbol{\Omega}$
Rashba	$\alpha(k_x\sigma_y - k_y\sigma_x)$	0
Rashba-Zeeman	$\alpha(k_x\sigma_y - k_y\sigma_x) + \Delta E/2\sigma_z$	Eq. (6)
2D Weyl node	$\hbar v(k_x\sigma_x + k_y\sigma_y)$	0
3D Weyl node	$\hbar v(k_x\sigma_x + k_y\sigma_y + k_z\sigma_z)$	$\pm\frac{\mathbf{k}}{2|\mathbf{k}|^3}$

the Rashba-like SS around non-TRIM may have benefits over the Rashba SS around TRIM owing to its tiny gap property protected by quasisymmetry.

In summary, we have addressed the physical origin of Rashba-like SS around non-TRIM based on symmetry analysis and DFT calculations. While at TRIM Kramers theorem ensures the double degeneracy of SS bands, the key feature of such Rashba-like SS around non-TRIM is the approximate degeneracy with a tiny SOC gap, as protected by SU(2) quasisymmetry. We further show that the combination of the little PG and orbital representation are both necessary conditions for such Rashba-like SS. In addition, we demonstrate that distinct from conventional Rashba SS defined at TRIM, Rashba-like SS around non-TRIM hosts a large Berry curvature, rendering them different material candidates for anomalous transports. Our work paves an avenue for understanding the ubiquitous Rashba physics, shedding light on the fundamental understanding of the general phenomena of spin splitting in crystals.

[1] G. Dresselhaus, Spin-orbit coupling effects in zinc blende structures, Phys. Rev. **100**, 580 (1955).

[2] E. I. Rashba, Properties of semiconductors with an extremum loop.1. Cyclotron and combinational resonance in a magnetic field perpendicular to the plane of the loop, Sov. Phys. Solid State **2**, 1109 (1960).

[3] H. Yuan, M. S. Bahramy, K. Morimoto, S. Wu, K. Nomura, B. J. Yang, H. Shimotani, R. Suzuki, M. Toh, C. Kloc, X. Xu, R. Arita, N. Nagaosa, and Y. Iwasa, Zeeman-type spin splitting controlled by an electric field, Nat. Phys. **9**, 563 (2013).

[4] C. Mera Acosta, L. Yuan, G. M. Dalpian, and A. Zunger, Different shapes of spin textures as a journey through the Brillouin zone, Phys. Rev. B **104**, 104408 (2021).

[5] L. L. Tao and E. Y. Tsymbal, Perspectives of spin-textured ferroelectrics, J. Phys. D **54**, 113001 (2021).

[6] A. Manchon, H. C. Koo, J. Nitta, S. M. Frolov, and R. A. Duine, New perspectives for Rashba spin-orbit coupling, Nat. Mater. **14**, 871 (2015).

[7] G. Bihlmayer, P. Noel, D. V. Vyalikh, E. V. Chulkov, and A. Manchon, Rashba-like physics in condensed matter, Nat. Rev. Phys. **4**, 642 (2022).

[8] S. Datta and B. Das, Electronic analog of the electro-optic modulator, Appl. Phys. Lett. **56**, 665 (1990).

[9] Q. Liu, Y. Guo, and A. J Freeman, Tunable Rashba effect in two-dimensional LaOBiS$_2$ films: Ultrathin candidates for spin field effect transistors, Nano Lett. **13**, 5264 (2013).

[10] V. M. Edelstein, Spin polarization of conduction electrons induced by electric current in two-dimensional asymmetric electron systems, Solid State Commun. **73**, 233 (1990).

[11] V. Mourik, K. Zuo, S. M. Frolov, S. R. Plissard, E. P. A. M. Bakkers, and L. P. Kouwenhoven, Signatures of Majorana Fermions in Hybrid Superconductor-Semiconductor Nanowire Devices, Science **336**, 1003 (2012).

[12] S. Nakosai, Y. Tanaka, and N. Nagaosa, Topological Superconductivity in Bilayer Rashba System, Phys. Rev. Lett. **108**, 147003 (2012).

[13] B. A. Bernevig, J. Orenstein, and S. C. Zhang, Exact SU(2) Symmetry and Persistent Spin Helix in a Spin-Orbit Coupled System, Phys. Rev. Lett. **97**, 236601 (2006).

[14] J. Schliemann, Colloquium: Persistent spin textures in semiconductor nanostructures, Rev. Mod. Phys. **89**, 011001 (2017).

[15] L. L. Tao and E. Y. Tsymbal, Persistent spin texture enforced by symmetry, Nat. Commun. **9**, 2763 (2018).

[16] H. J. Zhao, H. Nakamura, R. Arras, C. Paillard, P. Chen, J. Gosteau, X. Li, Y. Yang, and L. Bellaiche, Purely Cubic Spin Splittings with Persistent Spin Textures, Phys. Rev. Lett. **125**, 216405 (2020).

[17] X.-Z. Lu and J. M. Rondinelli, Discovery principles and materials for symmetry-protected persistent spin textures with long spin lifetimes, Matter **3**, 1211 (2020).

[18] J. H. Dil, Finding spin hedgehogs in chiral crystals, Physics **13**, 45 (2020).

[19] M. Sakano, M. Hirayama, T. Takahashi, S. Akebi, M. Nakayama, K. Kuroda, K. Taguchi, T. Yoshikawa, K. Miyamoto, T. Okuda *et al.*, Radial Spin Texture in Elemental Tellurium with Chiral Crystal Structure, Phys. Rev. Lett. **124**, 136404 (2020).

[20] G. Gatti, D. Gosálbez-Martínez, S. S. Tsirkin, M. Fanciulli, M. Puppin, S. Polishchuk, S. Moser, L. Testa, E. Martino, S. Roth *et al.*, Radial Spin Texture of the Weyl Fermions in Chiral Tellurium, Phys. Rev. Lett. **125**, 216402 (2020).

[21] Q. Liu, X. Zhang, H. Jin, K. Lam, J. Im, A. J. Freeman, and A. Zunger, Search and design of nonmagnetic centrosymmetric layered crystals with large local spin polarization, Phys. Rev. B **91**, 235204 (2015).

[22] C. Mera Acosta, A. Fazzio, and G. M. Dalpian, Zeeman-type spin splitting in nonmagnetic three-dimensional compounds, npj Quantum Mater. **4**, 41 (2019).

[23] K. Sakamoto, H. Kakuta, K. Sugawara, K. Miyamoto, A. Kimura, T. Kuzumaki, N. Ueno, E. Annese, J. Fujii, A. Kodama *et al.*, Peculiar Rashba Splitting Originating from the Two-Dimensional Symmetry of the Surface, Phys. Rev. Lett. **103**, 156801 (2009).

[24] M. Nagano, A. Kodama, T. Shishidou and T. Oguchi, A first-principles study on the Rashba effect in surface systems, J. Phys.: Condens. Matter **21**, 064239 (2009).

[25] T. Oguchi and T. Shishidou, The surface Rashba effect: A $k \cdot p$ perturbation approach, J. Phys.: Condens. Matter **21**, 092001 (2009).

[26] K. Yaji, A. Visikovskiy, T. Iimori, K. Kuroda, S. Hayashi, T. Kajiwara, S. Tanaka, F. Komori, and S. Shin, Coexistence of Two Types of Spin Splitting Originating from Different Symmetries, Phys. Rev. Lett. **122**, 126403 (2019).

[27] C. Guo, L. Hu, C. Putzke, J. Diaz, X. Huang, K. Manna, F.-R. Fan, C. Shekhar, Y. Sun, C. Felser, C. Liu, B. A. Bernevig, and P. J. W. Moll, Quasi-symmetry-protected topology in a semi-metal, Nat. Phys. **18**, 813 (2022).

[28] L. H. Hu, C. Guo, Y. Sun, C. Felser, L. Elcoro, P. J. W. Moll, C. X. Liu, and B. Andrei Bernevig, Hierarchy of quasisymmetries and degeneracies in the CoSi family of chiral crystal materials, Phys. Rev. B **107**, 125145 (2023).

[29] D. Vanderbilt, Soft self-consistent pseudopotentials in a generalized eigenvalue formalism, Phys. Rev. B **41**, 7892(R) (1990).

[30] P. Giannozzi, S. Baroni, N. Bonini, M. Calandra, R. Car, C. Cavazzoni, D. Ceresoli, G. L. Chiarotti, M. Cococcioni, I. Dabo *et al.*, QUANTUM ESPRESSO: A modular and open-source software project for quantum simulations of materials, J. Phys.: Condens. Matter **21**, 395502 (2009).

[31] J. P. Perdew, K. Burke, and M. Ernzerhof, Generalized Gradient Approximation Made Simple, Phys. Rev. Lett. **77**, 3865 (1996).

[32] M. Tinkham, *Group Theory and Quantum Mechanics* (Dover, Mineola, NY, 2003).

[33] R. Winkler, *Spin-Orbit Coupling Effects in Two-Dimensional Electron and Hole Systems*, Springer Tracts in Modern Physics (Springer, Berlin, 2003).

[34] P. Liu, J. Li, J. Han, X. Wan, and Q. Liu, Spin-Group Symmetry in Magnetic Materials with Negligible Spin-Orbit Coupling, Phys. Rev. X **12**, 021016 (2022).

[35] K. Sakamoto, T. Oda, A. Kimura, K. Miyamoto, M. Tsujikawa, A. Imai, N. Ueno, H. Namatame, M. Taniguchi, P. E. J. Eriksson, and R. I. G. Uhrberg, Abrupt Rotation of the Rashba Spin to the Direction Perpendicular to the Surface, Phys. Rev. Lett. **102**, 096805 (2009).

[36] D. Xiao, G. B. Liu, W. Feng, X. Xu, and W. Yao, Coupled Spin and Valley Physics in Monolayers of MoS_2 and Other Group-VI Dichalcogenides, Phys. Rev. Lett. **108**, 196802 (2012).

[37] L. L. Tao and E. Y. Tsymbal, Spin-orbit dependence of anisotropic current-induced spin polarization, Phys. Rev. B **104**, 085438 (2021).

[38] K. Yang, Y. Wang, and C.-X. Liu, Momentum-Space Spin Antivortex and Spin Transport in Monolayer Pb, Phys. Rev. Lett. **128**, 166601 (2022).

[39] G. L. Bir and G. E. Pikus, *Symmetry and Strain-Induced Effects in Semiconductors* (Wiley, New York, 1974).

[40] S. Vajna, E. Simon, A. Szilva, K. Palotas, B. Ujfalussy, and L. Szunyogh, Higher-order contributions to the Rashba-Bychkov effect with application to the Bi/Ag(111) surface alloy, Phys. Rev. B **85**, 075404 (2012).

[41] L. L. Tao, T. R. Paudel, A. A. Kovalev, and E. Y. Tsymbal, Reversible spin texture in ferroelectric HfO_2, Phys. Rev. B **95**, 245141 (2017).

[42] I. Appelbaum and P. Li, Electrons, holes, and spin in the IV-VI monolayer four-six-enes, Phys. Rev. B **94**, 155124 (2016).

[43] Y. M. Xie, X. J. Gao, X. Y. Xu, C. P. Zhang, J. X. Hu, J. Z. Gao, and K. T. Law, Kramers nodal line metals, Nat. Commun. **12**, 3064 (2021).

[44] D. Di Sante, P. Barone, R. Bertacco, and S. Picozzi, Electric control of the giant Rashba effect in bulk gete, Adv. Mater. **25**, 313 (2013).

[45] L. L. Tao and J. Wang, Strain-tunable ferroelectricity and its control of Rashba effect in $KTaO_3$, J. Appl. Phys. **120**, 234101 (2016).

[46] L. G. D. da Silveira, P. Barone, and S. Picozzi, Rashba-Dresselhaus spin-splitting in the bulk ferroelectric oxide $BiAlO_3$, Phys. Rev. B **93**, 245159 (2016).

[47] J. Gosteau, R. Arras, P. Chen, H. J. Zhao, C. Paillard, and L. Bellaiche, Spin-orbit effects in ferroelectric $PbTiO_3$ under tensile strain, Phys. Rev. B **103**, 024416 (2021).

[48] A. Narayan, Class of Rashba ferroelectrics in hexagonal semiconductors, Phys. Rev. B **92**, 220101(R) (2015).

[49] F. Reis, G. Li, L. Dudy, M. Bauernfeind, S. Glass, W. Hanke, R. Thomale, J. Schaer, and R. Claessen, Bismuthene on a SiC substrate: A candidate for a high-temperature quantum spin Hall material, Science **357**, 287 (2017).

[50] D. Xiao, M. C. Chang, and Q. Niu, Berry phase effects on electronic properties, Rev. Mod. Phys. **82**, 1959 (2010).

[51] M. Papaj and L. Fu, Magnus Hall Effect, Phys. Rev. Lett. **123**, 216802 (2019).

[52] D. Mandal, K. Das, and A. Agarwal, Magnus Nernst and thermal Hall effect, Phys. Rev. B **102**, 205414 (2020).

[53] P. Kapri, B. Dey, and T. K. Ghosh, Magnus spin Hall and spin Nernst effects in gapped two-dimensional Rashba systems, Phys. Rev. B **106**, 035420 (2022).

[54] K. Momma and F. Izumi, VESTA 3 for three-dimensional visualization of crystal, volumetric and morphology data, J. Appl. Crystallogr. **44**, 1272 (2011).